SLAMMING AND WATER SHIPPING ON A VLFS WITH SHALLOW DRAFT

M. Greco
INSEAN, The Italian Ship Model Basin
Via di Vallerano 139, 00128, Roma, Italy
Email: m.greco@insean.it

M. Landrini
INSEAN, The Italian Ship Model Basin
Via di Vallerano 139, 00128, Roma, Italy
Email: maulan@waves.insean.it

O.M. Faltinsen
Dept. Marine Technology
NTNU, Trondheim, Norway
Email: oddfal@marin.ntnu.no

Floating airports consisting of barge-type Very Large Floating Structures (VLFS) have been proposed in Japan and extensively investigated by linear hydroelastic theory. Though in practical cases both bottom slamming and green water should be of concern, there are limited studies available, *i.e.* [9] and [6]. In the following, a two-dimensional fully-nonlinear wave tank, solved numerically by BEM, is applied to green water and bottom slamming on a restrained VLFS with shallow draft. A local analytical solution is introduced to cope with small angles between impacting free surface and bottom. Air cushions appearing during bottom events are dealt with by assuming quasi-steady adiabatic evolution of the entrapped air.

Model problem A two-dimensional problem for incompressible water in irrotational motion is assumed. Surface tension is neglected. In this framework, we model numerically a wave maker generating waves incident on a barge-type VLFS with shallow draft and finite freeboard (see Fig. 1). Details of the numerical modelling are given in [4]. The

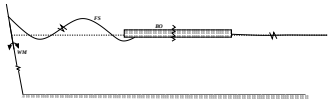

case	H/D	$T(g/D)^{1/2}$
1	3·2	21·0
2	3·4	31·1
3	3·6	19·7
4	4·1	21·5
5	4·9	21·5
6	6·3	25·6
7	6.·3	21·7

Figure 1. Left: Analyzed two-dimensional problem. Right: Studied cases. T = wave period. H = incident wave height. g = acceleration of gravity.

freeboard-to-draft ratio is $f/D = 3{\cdot}7$ and it is representative for a barge-type airport. The length-to-draft ratio is $L/D = 120$, smaller than a typical value of about 3000. Since in our case the body is restrained from moving, this difference is believed unimportant for studying details of the flow at the front edge. However, results can be influenced by VLFS motions, which require the whole length of the airport to be considered. The wave maker is located at $240D$ from the front edge of the body. The fluid depth is $60D$, which implies infinite fluid depth from a hydrodynamic point of view. A numerical wave beach is introduced starting at a distance $240D$ past the platform to limit the fluid domain and avoid unphysical wave reflection from the end of the computational domain.

Air cushions generated during bottom slamming are dealt with by neglecting the air flow and assuming an evolution of the air pressure, *i.e.* $p = p_a[\mathrm{Vol}_0/\mathrm{Vol}(t)]^\gamma$, where p_a is the atmospheric pressure, Vol_0 is the initial volume at closure of the air cushion and $\gamma = 1{\cdot}4$.

General aspects In the numerical simulations, the wave-maker motion has been prescribed to generate regular incoming waves. The wave-body interaction has been studied during the transient until nearly steady-state conditions are reached.

In all cases considered, listed in the table of Fig. 1, bottom slamming is observed. In particular, it starts from the front deck edge and is characterized by air-cavity entrapment. Figure 2 shows an example: the angle between the free surface and body appears generally quite small, varying from ten to very few degrees. The first bottom impact is much smaller than the second and the third ones which are practically the same, showing that almost steady-state conditions are reached.

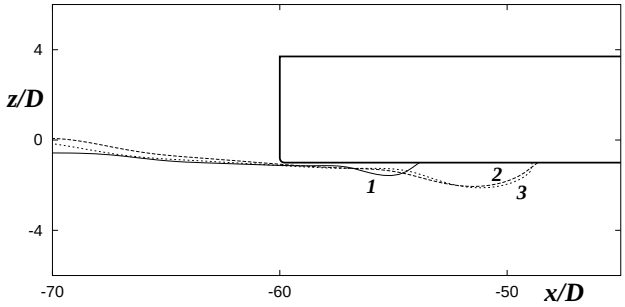

Figure 2. Free-surface profiles for case 3. The free-surface configurations are enumerated as the time increases.

For some cases, the combination of long and sufficiently high incoming waves determined also water-shipping occurrence. An example is reported in Fig. 3, where also bottom slamming occurs.

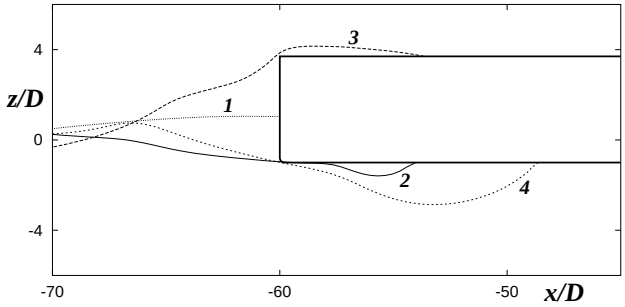

Figure 3. Free-surface profiles for case 5.

Maximum bottom emergence Once the draft is exceeded by the water, a portion of the VLFS bottom becomes dry. The maximum bottom emergence l_d, Fig. 4, is a measure of the bottom area affected by slamming. The experimental values from [9] of $l_{d\,max}$ for $T\sqrt{g/D} = 19{\cdot}06$ and $D = 0{\cdot}27$ m are presented as function of H/D and compared with the present numerical simulations for the indicated values of $T\sqrt{g/D}$.

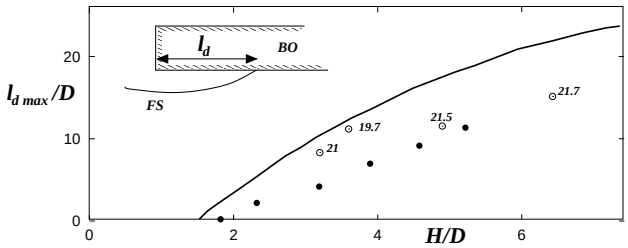

Figure 4. Maximum bottom emergence $l_{d\,max}$ by two-dimensional experiments, ●, and linear theory, solid line, from [9] for the highest-rigidity case (model B) and $T(g/D)^{1/2} = 19{\cdot}06$. Our predictions for restrained model, ○.

Two global rigidities are considered in [9]. The case shown (model-B) corresponds to the highest rigidity, and the measured vertical-motion amplitudes were the smallest and less than 15% of the incident-wave amplitude. For this case, similar to our numerical predictions, [9] reported formation of air cushions during bottom slamming. The theoretical result from [9], solid line, is also reported. It is based on linear hydroelastic theory and on assuming bottom-clearance occurrence when the amplitude of the dynamic pressure at a specific location is larger than the hydrostatic bottom pressure. These results for dynamic-pressure amplitude along the VLFS indicate that closed cavities similar as those shown in Figs. 2-3 by fully-nonlinear simulations cannot be predicted by that linear theory. Our prediction of maximum bottom emergence agrees better with the experiments than the linear theory does. However, the VLFS is moving in the experiments while our model is restrained. This influences the results. For instance, experiments on a model with smaller global rigidity and larger vertical platform motions at the front end (model-A) showed that air cushions did not occur, [9].

Bottom slamming with small relative bottom-free surface angle Typically, during bottom slamming, the water hits the lower front edge of the VLFS with very small angles between the free surface and the bottom and very rapid changes of the wetted area next to the front edge occur. In such cases, near the first impact location, the free surface can be approximated by a straight line. In order to deal with this situation, a local analytical solution has been introduced, [3]. The analytical solution considers the impact of a flat free surface against the bottom surface. The initial impact position is the front edge. Slope and impact velocity of the free surface at the impact position follow from the fully-nonlinear simulation before impact occurrence. The impact flow is locally solved similarly as [7] and patched with an outer fully-nonlinear simulation. Details will be given at the Workshop.

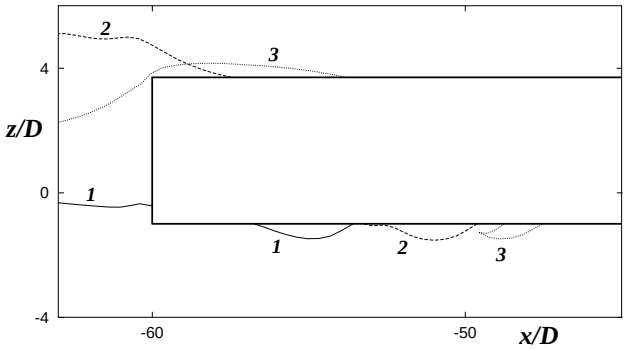

Figure 5. Full-scale evolution of the cavity, $D = 1{\cdot}5$ m, for case 5.

Figure 5 shows water evolution after the impact occurrence. The cavity deforms and moves under the influence of the surrounding flow. Finally it tends to detach from the structure and collapse. We cannot predict the collapse of the cavity into bubbles. This happens before a new water rundown with draft exceedance occurs. The cavity evolution affects the loads on the VLFS bottom but is unimportant for flow details in front of the front deck edge. This is confirmed by comparing the free-surface evolution obtained by cutting the free-surface portion coinciding with the cavity surface after the bottom impact. This means, if steady-state conditions are wanted one can study simply the bottom impact occurring in such circumstances and cut the previous cavities. This has been made for instance in the simulations shown in Figs. 2 and 3.

The evolution of the cavity pressure relative to p_a during the first bottom impact is given in the top plot of Fig. 6 for case 5. The results refer to full scale, $D = 1{\cdot}5$ m, and model scale, $D = 0{\cdot}027$ m, adopted in the experiments [9]. In both cases an oscillating pressure is found but the oscillation period reduces with the scale as well as the maximum pressure. The minimum pressure remains almost unchanged. From the results, the cavity pressure does not scale with Froude number. If the experimental values were Froude scaled, the experiments would predict larger cavity volumes more highly vibrating than in reality. Further, Froude scaling of $p - p_a$ from $D = 0{\cdot}027$ m to $D = 1{\cdot}5$ m gives about 9 times the value obtained numerically for $D = 1{\cdot}5$ m, *cf.* Fig. 6. Bottom plot

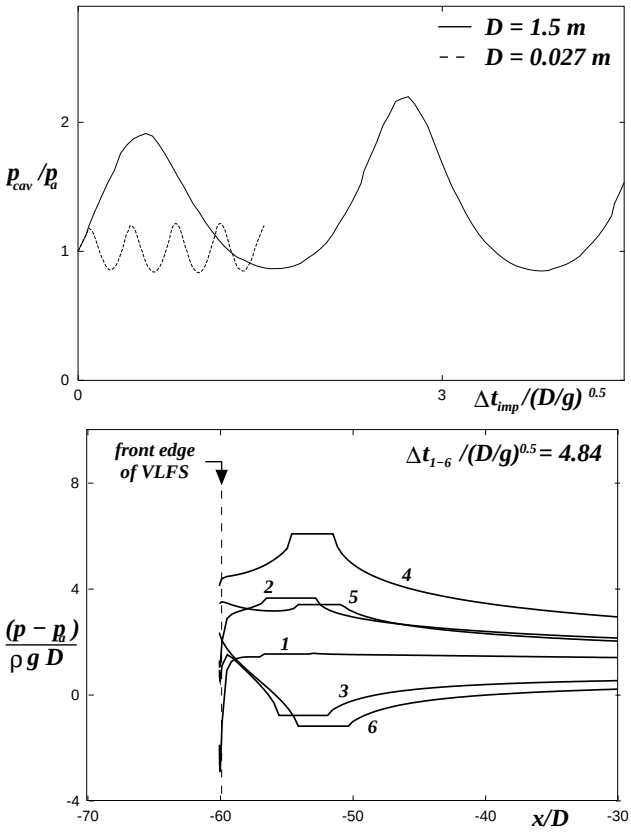

Figure 6. First bottom impact for case 5. Top: pressure evolution in the cavity; solid line: $D = 1{\cdot}5$ m (full scale), dashed line: $D = 0{\cdot}027$ m (model scale, [9]). Bottom: pressure evolution along the VLFS bottom for $D = 1{\cdot}5$ m (full scale). Δt_{1-6}= time interval between configurations numbered 6 and 1.

of Fig. 6 shows the time evolution of the bottom pressure after the impact in the full scale case. There is a large negative value of $p - p_a$ at the front edge at the first time instant shown, indicated as 1. This is associated with the quadratic velocity term in Bernoulli equation and is due to high cross-flow velocity at the edge. Since vortex shedding occurs in reality, we should be skeptical about the quantitative level of the negative $p - p_a$. The pressure is above cavitation pressure. The structural effect of the pressure loading will be discussed later.

Water shipping on the deck Following [4], we have modelled the water shipping on the deck of the VLFS structure. The numerical amount of shipped water obtained for cases 5 and 6 is presented in Fig. 7 and compared with an empirical formula for estimating water volume of waves overtopping on a vertical breakwater, [8], reported in the same figure. The time t' is referred to the starting of the water shipping, and $[Z(t') - Z_0]$ represents the instantaneous freeboard exceedance. As proposed in [8], we used $m = 0{\cdot}5$. The numerical and experimental values are in reasonable agreement. However, since the mass flux of water through a vertical plane coinciding with the front side of the platform determines the water volume on the deck, the wave period

$$Q = 2\mathrm{m}\sqrt{2g}/3 \int_0^t [Z(t') - Z_0]^{3/2} \mathrm{d}t'$$

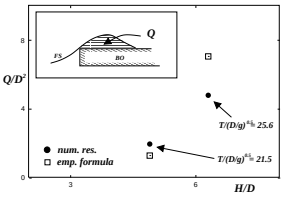

Figure 7. Amount of water overtopping the VLFS structure in cases 5 and 6. The numerical results are compared with those from the empirical formula reported from [8].

must be an important parameter in addition to $[Z(t') - Z_0]$. In [6], all the experimental results for regular and irregular waves with different periods are compared against the empirical formula with m= 0·7. A large scatter occurred documenting that the approach is not sufficient for quantitative predictions.

Run-down and turning of the free surface around front edge After the run-down phase of the water along the front side, the free surface will turn rapidly around the front edge. This is associated with vortex separation from the sharp edge. The latter effect is neglected in our analysis. In order to facilitate the numerical simulations, the front edge has been rounded with a radius $R = 0{\cdot}2D$. This is relatively large in the scale of the local impact, however comparisons between free-surface evolutions after the bottom impact with $R = 0{\cdot}2D$ and $R = 0{\cdot}01D$ did not show substantial differences.

Two main types of bottom turning have been observed. In one case, the free surface near the front deck edge is relatively flat. This occurs during the transient and when the wave-body interaction is not characterized by large nonlinearities. In the other case, the free surface running down the structure detaches from the body as thin layer of fluid with small angle between free surface and structure. This evolution is reported in Fig. 8. The free surface has a very small curvature radius just after it has turned around the front edge of the bottom. We do not have experimental evidence

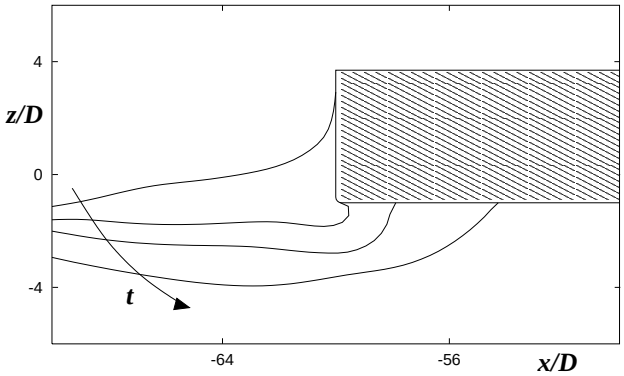

Figure 8. Turning phenomenon for case 5 and $R/D = 0{\cdot}2$.

for this for a VLFS. However, Baarholm [1] presented two-dimensional experimental results for wetdeck slamming that showed a similar behaviour.

The turning of the free surface around the front edge during the run-down is associated with the occurrence of local negative pressures $p - p_a$ due to high flow velocities, similarly to the turning associated with the water run-up after the bottom impact. Other phases of the flow evolution are also connected with negative $p - p_a$. These have been indicated from experiments in [9] as reported in the top left plot of Fig. 9, showing the pressure time evolution at the location P-1 at about 1·48D from the front edge. Here $p = -2{\cdot}7$

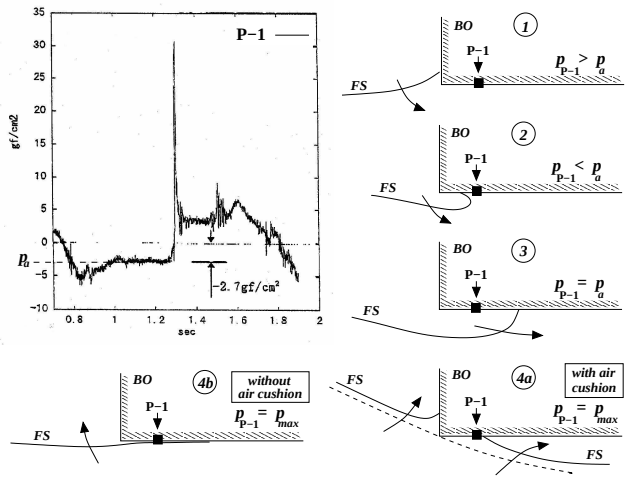

Figure 9. Pressure measurements from [9] at location P-1 ($D = 0{\cdot}027$ m) with Model A having smallest rigidity ($T = 1{\cdot}05$ s, $H = 13{\cdot}8$ cm). Frames 1-4b give the physical interpretation of the experimental findings.

gf/cm^2 ($\sim$ 265 Pa) corresponds to the atmospheric pressure p_a since the hydrostatic value has been subtracted from the pressure record. As we can observe, at the beginning of the shown time evolution, the pressure reduces, gets negative values for about 0·2 s, then it increases becoming atmospheric for about 0·3 s and after that the maximum value is reached. These stages can be explained through the sketches 1-4 in the same figure. Before the bottom turning of the water, pressure is greater than p_a (sketch 1). After the turning, the free surface is locally characterized by high curvature and propagates along the bottom approaching location P-1. This "water-exit" phase is associated with negative pressures mainly due to the positive values of $\partial\varphi/\partial t$ (sketch 2). In [9], it is speculated that the negative pressures were due to surface tension. It is true that surface tension may affect flows with high cur-

vature of the free surface. However, the main effect is due to fluid-acceleration expressed in terms of $\partial\varphi/\partial t$. Once the water front leaves P-1 this location remains dry, the pressure becoming atmospheric (sketch 3). This lasts until the bottom impact occurs, affecting P-1 and determining $p = p_{max}$. This can be either associated with air cushion formation, starting from the front edge (sketch 4a), or can occur without air entrapment, initiating from the intersection of the free surface with the bottom (sketch 4b). The latter situation occurred during the shown experimental case.

Slamming-load effects Structural effects of the bottom-impact loading, *cf.* Fig. 6, will be assessed by hydroelastic analysis, *e.g.* [2]. The stiffened bottom plating with longitudinal stiffeners between two transverse stiffeners is modeled by an equivalent beam. Only the equivalent beam next to the front edge is considered. The following hydrodynamic simplifications are made. The excitation pressure assumes a rigid body. The pressure due to the beam oscillations is estimated by neglecting the air cushion. The case study considers structural mass per unit length and breadth 240·7 Kg/m^2, beam bending stiffness $EI \simeq 27{\cdot}5$ MNm^2 and a distance from the neutral axis to where maximum stresses occur $z_a \simeq 0{\cdot}23$ m. The beam has a length $L_b = 5$ m and it is clamped at the ends.

The time evolution of maximum tension and compression stresses at the end position is shown in Fig. 10 together with the pressure inside the cavity. For $t \geq 0{\cdot}75$ s the beam is fully wetted. Results are given both for a dry-mode solution, solid lines, and for an approximate hydroelastic theory, dashed lines, where the structural mass is corrected by an added-mass term. On a large time scale, the stress evolution follows the cavity pressure in a quasi-steady manner. The high-frequency oscillations are related to first-mode vi-

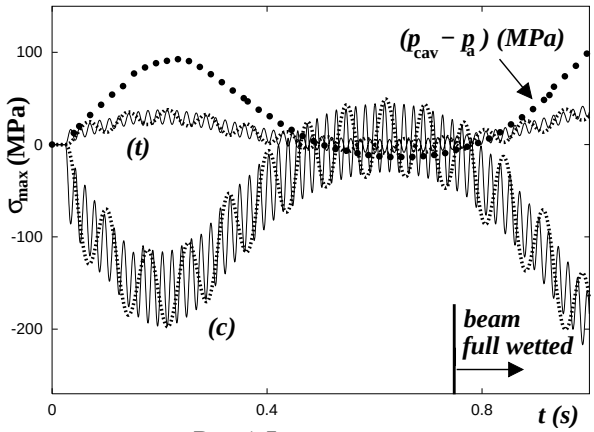

Figure 10. Full-scale, $D = 1{\cdot}5$ m, maximum tension (t) and compression (c) stresses on the beam during the first bottom impact in case 5. Solid lines: dry-mode response. Dashed lines: approximate hydroelastic response. •: cavity pressure. $t = 0$ s is the impact time. For $t \geq 0{\cdot}75$ s the beam is fully wetted.

brations, with lower frequency in case of the approximate hydroelastic theory (dry natural period$\sim 0{\cdot}018$ s, approximate wet natural period$\sim 0{\cdot}073$ s). In this case study, the hydroelastic effects are not dominant. The maximum absolute value of the stress is ~ 200 MPa and it should for instance be related to yield stress 320-360 MPa for high strength steel (NK standard).

During the second bottom impact, *cf.* top plot of Fig. 11, the left edge of the cavity, configuration 1, moves rightwards in the form of a jet of liquid, configurations 2 and 3, progressively detaching the cavity from the VLFS bottom. In the numerical simulation for model scale, $D = 0{\cdot}027$ m, shown in the bottom plot, the cavitation number is large enough to prevent jet-flow formation. This would suggest the inadequacy of model tests to evaluate the possible structural failure. The structural consequences of these fluid-flow differences will be further discussed at the Workshop.

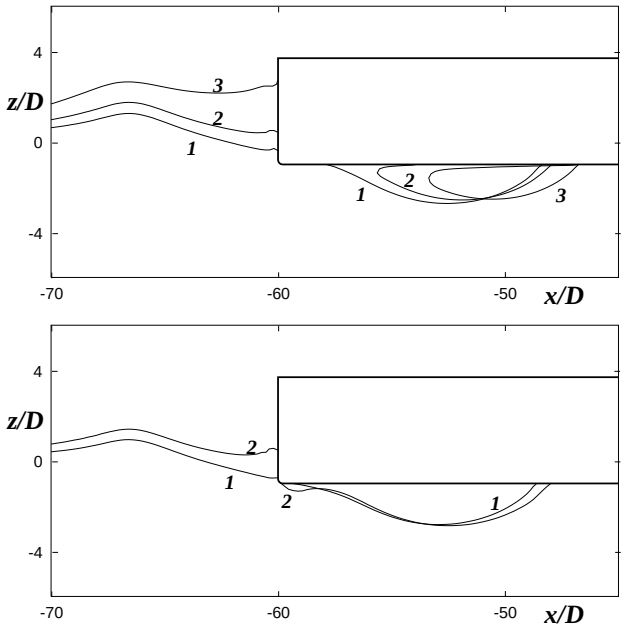

Figure 11. Second bottom impact for case 5, free-surface configurations. Top: full scale, $D = 1{\cdot}5$ m. Bottom: model scale, $D = 0{\cdot}027$ m.

INSEAN research activity is supported by the Italian *Ministero per le Infrastrutture e Trasporti* through INSEAN Research Program 2003-05.

REFERENCES

[1] R.J. Baarholm, Theoretical and Experimental Studies of Wave Impact underneath Decks of Offshore Platforms, Ph. D. Thesis, Dept. Marine Hydrodynamics, NTNU, Trondheim, Norway, 2001.

[2] O.M. Faltinsen, Hydroelastic slamming, J. Mar. Sci. Technol., Vol. 5, No. 2, 2001.

[3] O.M. Faltinsen, M. Landrini and M. Greco, Slamming in marine applications, submitted to *J. Engng. Math.* (2003).

[4] M. Greco, A Two-dimensional Study of Green-Water Loading, Ph. D. Thesis, Dept. Marine Hydrodynamics, NTNU, Trondheim, Norway, 2001.

[5] M. Greco, O.M. Faltinsen and M. Landrini, Basic Studies of Water on Deck, Proc. 23rd Symp. on Naval Hydrod., Val de Reuil, National Academy Press, Washington D.C., 2000.

[6] Y. Takaishi, K. Minemura and K. Masuda, Experimental study on relative motion and shipping water of mega-fbat structure, OMAE98-4335, Lisbon, Portugal, 1998.

[7] H. Wagner, Uber stoss- und gleitvorgange an der oberfhche von flssigkeiten, ZAMM 12(4), pp.192-235, 1932.

[8] H. Kikkawa, H. Shiagai and T. Kono, Fundamental Study on Wave Overtopping Sea Dikes, In: *Proc. Coastal Engineering*, JSCE, pp.118-122, 1967.

[9] H. Yoshimoto, K. Ohmatsu, S. Ohmatsuandi and T. Ikebuchi, Slamming load on a very large fbating structure with shallow draft, J. Mar. Sci. Technol., Vol. 2, pp. 163-172, 1997.

Question by : M. Tulin
Congratulations on treating this leading edge problem, which I think is very important in connection with the interaction of waves with floating mass. Did you allow the trapped air to compress, what would be the influence of air escaping at the side edges?

Author's reply:
Yes we allowed the trapped air to compress. In particular, we treated the air as an ideal gas subjected to an adiabatic process and assumed uniform the cavity pressure. In this way equation

$$\frac{p(t)}{p_a} = \left(\frac{V_0}{V(t)} \right)^{1.4}$$

applies, $p(t)$ and $V(t)$ being the instantaneous pressure and volume of the cavity and p_a and V_0 the atmospheric pressure and the initial volume at the cavity closure, respectively.
If three-dimensional effects matter so that the air can escape laterally at the side edges it is not obvious how the corresponding loads acting on the VLFS would be changed. On one hand, the air compression would be reduced by the escaping process causing a smaller pressure in the cavity with respect to the two-dimensional case. On the other hand, smaller values of the cavity pressure would support the development of jet flows at the intersection between the cavity and the VLFS bottom. These would cause higher structural loads.

Question by : M. Kashiwagi
I was thinking that your method is based on a fully nonlinear BEM, but you said that the free-surface boundary condition is simply phi = 0 on z =0. Is this correct?

Author's reply:
Our method is based on a fully nonlinear BEM. Condition $\Phi = 0$ on $z = 0$ is applied in the local problem (near the fore edge of the VLFS, see the abstract) to handle the impact phenomena. More in detail, when impact occurs we divide the velocity potential into two parts, one of those related to the impact phenomenon, say Φ_i. It is only the velocity potential caused by the impact that is assumed zero on $z = 0$ ($\Phi_i = 0$) initially and locally at the front edge. This condition implies that the impact phenomenon does not affect the velocity potential on the free surface, so that in the inner region the free surface velocity potential after the impact is obtained through the BEM solution.
